

Molecular Motion in a Spreading Precursor Film

Hui Xu,¹ David Shirvanyants,¹ Kathryn Beers,² Krzysztof Matyjaszewski,²
Michael Rubinstein,¹ and Sergei S. Sheiko^{1,*}

¹Department of Chemistry, University of North Carolina at Chapel Hill, North Carolina 27599-3290, USA

²Department of Chemistry, Carnegie Mellon University, 4400 Fifth Avenue, Pittsburgh, Pennsylvania 15213, USA
(Received 3 June 2004; published 10 November 2004)

Spreading of a polymer drop on a solid substrate was monitored with molecular resolution. Three characteristic rates, i.e., the spreading rate of the precursor film $D_{\text{spread}} = (3.9 \pm 0.2) \times 10^3 \text{ nm}^2/\text{s}$, the flow-induced diffusion rate of molecules within the film $D_{\text{induced}} = 1.3 \pm 0.1 \text{ nm}^2/\text{s}$, and the thermal diffusion coefficient of single molecules $D_{\text{therm}} \leq 0.10 \pm 0.03 \text{ nm}^2/\text{s}$, were independently measured. Since $D_{\text{spread}} \gg D_{\text{induced}}$, the plug flow of polymer chains was identified as the main mass-transport mechanism of spreading with an insignificant contribution from the molecular diffusion.

DOI: 10.1103/PhysRevLett.93.206103

PACS numbers: 68.08.Bc, 36.20.-r, 68.15.+e, 68.37.-d

Quite often we see a liquid drop spreading on a solid surface to give a thin film of finite thickness. This everyday phenomenon plays a key role in many important processes, such as oil recovery, lubrication, painting, and mass transport through the lung airways. The macroscopic behavior of spreading drops is well understood [1–3], yet our understanding of the molecular mechanism of spreading remains incomplete and controversial [4–7]. This lack of microscopic knowledge is now an urgent problem limiting development in microfluidic devices and nanoscale machines, whose characteristic time and length scales are approaching those of individual molecules. Here we report on molecular visualization of the spreading process of polymer-melt drops. For the first time, it is possible to measure simultaneously the displacement of the contact line and displacements of individual molecules within the precursor film. The mass-transport mechanism was clearly identified as plug flow, i.e., collective sliding of polymer chains with an insignificant contribution from the molecular diffusion.

The spreading of a drop begins with the formation of a thin precursor film [8] [Fig. 1(a)]. This is then followed by a macroscopic drop which has a terraced foot assigned to concurrent sliding of monolayers stacked on top of one another [9,10]. Unlike the drop radius, which follows the Hoffman-Tanner relation $R(t) \sim t^{1/10}$, the precursor-film length obeys the diffusionlike law $L(t) \sim \sqrt{t}$. Both the precursor film and the molecular terraces belong to the generic features of spreading observed by ellipsometry for different types of fluids [10–13]. However, because of low resolution ($\sim 30 \mu\text{m}$), ellipsometry fails to resolve questions on the mechanisms of mass transport and energy dissipation in the liquid layers. The unique advantage of atomic force microscopy (AFM) is that it allows visualization of molecules [14–18]. Although this advantage was immediately recognized, the first AFM measurements of spreading drops did not attain molecular resolution [19,20]. Investigation of the molecular motion

requires visualization of molecules both in space and in time. We solved this problem through the use of model brush molecules [Fig. 1(b)].

The model properties of cylindrical brushes are associated with densely grafted side chains that aid in the visualization process in four ways. First, adsorbed side chains separate the molecular backbones. Depending on the side-chain length and the grafting density, the intermolecular distance varies from 5 to 60 nm [15]. Second, because of the high grafting density there is a fraction of side chains that aggregate along the backbone above the substrate plane [21] [Fig. 2(c)]. The ridge of the desorbed

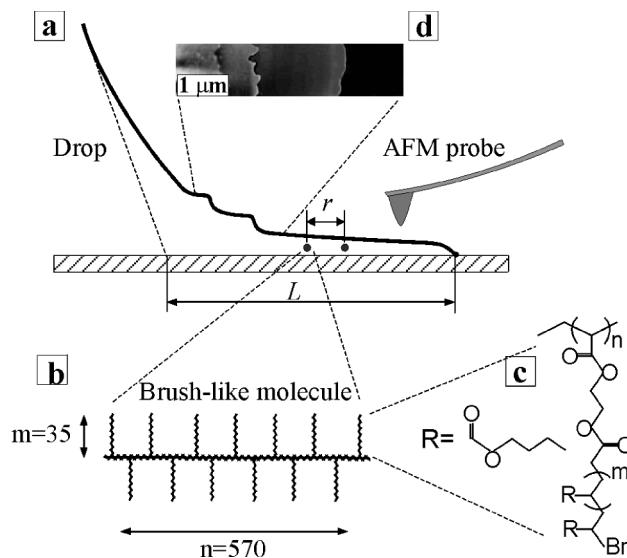


FIG. 1. (a) A microscopic drop of a polymer-melt (volume $\sim 1 \text{ nl}$, radius $\sim 100 \mu\text{m}$) was scanned by AFM to measure the displacement L of the precursor-film edge and the distance r between the molecules within the film. The polymer melt is composed of (b) cylindrical brush molecules with (c) poly(*n*-butyl acrylate) side chains. (d) At later stages of spreading on mica one observed monolayer terraces at the foot of the drop with a thickness of 5 nm.

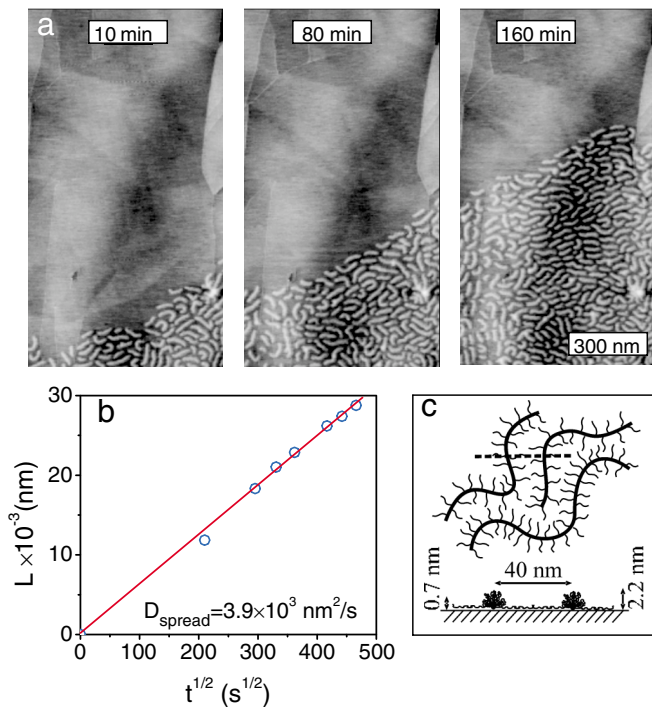


FIG. 2 (color online). (a) AFM monitors sliding of the precursor monolayer of PBA brushes on the HOPG surface. The images were captured at different spreading times: 10, 80, and 160 min. (b) Mean displacement of the film edge gives the spreading rate $D_{\text{spread}} = (3.9 \pm 0.2) \times 10^3 \text{ nm}^2/\text{s}$. (c) The cartoon shows organization of brush molecules within the monolayer. Backbones with a ridge of desorbed side chains provide height contrast, while the spacing between the molecules is determined by adsorbed side chains.

side chains provides height contrast. Third, the repulsion of the adsorbed side chains increases the stiffness of the backbone. Depending on the side-chain length, the apparent persistence length ranges from 10–500 nm [15] enabling measurements of molecular curvature. Fourth, the number of monomeric contacts with the substrate (per unit length of the backbone) increases with the side-chain length and the grafting density. This depresses mobility of adsorbed molecules and facilitates their temporal resolution.

In this work we studied brush molecules with a polymethacrylate backbone and of poly(*n*-butyl acrylate) (PBA) side chains [Fig. 1(c)] prepared by atom transfer radical polymerization [22]. The number of the average degree of polymerization of the backbone is $n = 570 \pm 50$, the side chains have a degree of polymerization of $m = 35 \pm 5$, and the grafting density is 1; i.e., every monomeric unit of the backbone contains one side-chain. A drop of PBA brushes (volume $\sim 1 \text{ nl}$, radius $\sim 100 \mu\text{m}$) was deposited on the surface of highly oriented pyrolytic graphite (HOPG) at a controlled relative humidity of 25% and a temperature of 25 °C. At room temperature, the material is liquid ($T_g = -50^\circ\text{C}$) with a zero-shear vis-

cosity $\eta_0 = 8340 \text{ Pa}\cdot\text{s}$. Once the drop touched the substrate, a thin precursor film was observed growing from the foot of the drop. In addition, monomolecular terraces developed at the foot of the drop [Fig. 1(d)]; as many as 6 terraces were detected consistent with the terraced-droplet model [9]. The motion of the terraces is the subject of ongoing research, while this work is focused on the precursor film.

The motion of the precursor film was monitored by AFM in different regions of the precursor film located along different radial directions with respect to the drop center. In total, ten drops were studied to ensure reproducibility and accurate data averaging. Figure 2(a) shows three snapshots captured at the edge of the growing film. The important outcome of this experiment is the simultaneous observation of both the displacement of the film edge and the motion of individual molecules within the film. The time dependence of the film length in Fig. 2(b) obeys the diffusionlike law $L(t) = \sqrt{D_{\text{spread}}t}$ at a spreading rate of $D_{\text{spread}} = (3.9 \pm 0.2) \times 10^3 \text{ nm}^2/\text{s}$.

In addition to the film displacement, the AFM images provide information on the molecular structure of the precursor film. Each brush molecule is visualized as a flat wormlike object with a thickness of $h = 0.7\text{--}2.2 \text{ nm}$ and a width of $d = 40 \pm 3 \text{ nm}$ [Fig. 2(c)]. The $0.7 \pm 0.1 \text{ nm}$ thickness corresponds to the area between the backbones which is covered by adsorbed side chains, while the $2.2 \pm 0.2 \text{ nm}$ thickness is measured at the ridge of desorbed side chains. By analyzing an ensemble of 300 molecules, we determined a number average contour length of $L_n = 105 \pm 5 \text{ nm}$ and a polydispersity index of $L_w/L_n = 1.17$. From the backbone curvature [14] we determined a persistence length of $l_p = 112 \pm 10 \text{ nm}$. Since $l_p \approx L_n$, one deals here with wormlike molecules.

Through use of AFM we also were able to monitor temporal changes in position, orientation, and conformation of individual molecules [Fig. 3(a)]. We monitored a group of 100 molecules to record the coordinates of the center of mass of the group $R_{cm}(t)$ along with the coordinates of the individual molecules $R_i(t)$ and $r_i(t) = R_i(t) - R_{cm}(t)$ relative to the substrate and to the center of mass, respectively. Figure 3(b) depicts the trajectory of the center of mass and the trajectories of three molecules from the group. In the frame of the substrate, the trajectories demonstrate a convective flow along the spreading direction. However, in the frame of the precursor-film molecules move in a random-walk fashion which will be later identified as flow-induced diffusion. Figure 3(c) depicts the time dependence of the mean-square displacement $\langle r^2(t) \rangle = 4D_{\text{induced}}t$ with a diffusion coefficient of $D_{\text{induced}} = 1.3 \pm 0.1 \text{ nm}^2/\text{s}$, which is 3 orders of magnitude lower than the spreading rate D_{spread} of the film edge. In other words, during $\sim 1 \text{ h}$ individual molecules separate by a distance of 100 nm (~ 1 molecular size) as the film moves a distance of $\sim 3 \mu\text{m}$ (~ 30 molecular sizes).

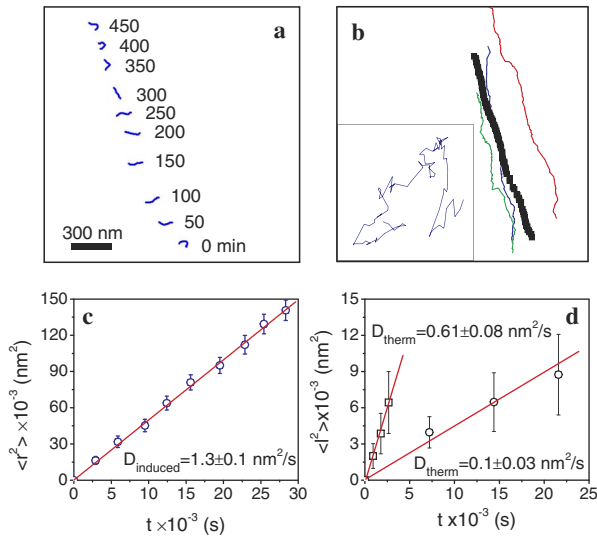


FIG. 3 (color online). (a) Animation of one of the spreading molecules demonstrates different modes of the molecular motion including translation of the center of mass, chain rotation, and fluctuations in the backbone curvature. The numbers indicate the observation time during the spreading process. (b) The trajectories of the center of mass of a group of 100 molecules (bold line) along with individual trajectories of three molecules (thin lines). The inset shows the path of one of the molecules in the frame of the precursor film by plotting the molecular trajectory relative to the center of mass of the group. (c) Mean-square intermolecular displacement $\langle r^2 \rangle = 4D_{\text{induced}}t$ was averaged for 100 molecules to determine the molecular diffusion coefficient $D_{\text{induced}} = 1.3 \pm 0.1 \text{ nm}^2/\text{s}$. (d) Translational diffusion of 80 single brush molecules was monitored by AFM via interruptive scanning to determine two diffusion coefficients $D_{\text{therm}} = 0.61 \pm 0.08 \text{ nm}^2/\text{s}$ and $D_{\text{therm}} = 0.10 \pm 0.03 \text{ nm}^2/\text{s}$ at 10-minute (\square) and 2-hour (\circ) intervals between the consecutive scans, respectively.

As such, the mass transport is identified as plug flow with insignificant contribution from the diffusive motion.

Brush molecules also demonstrated rotational motion. The time correlation function of the end-to-end vector $u(t)$ follows the exponential decay $\langle u(t)u(0) \rangle \propto \exp(-t/\tau_r)$ with a rotational relaxation time of $\tau_r = 5.3 \times 10^4 \text{ sec}$ ($\sim 10 \text{ h}$). Therefore, both the translation and rotation of brush molecules in the frame of the precursor film are much slower than the plug flow.

The diffusive motions are consistent with the fluid nature of the precursor film; however, they cannot be ascribed to thermally induced self-diffusion. The weak contribution of the thermal diffusion to the spreading process became evident from the Brownian motion of single molecules prepared by adsorption from a dilute solution (HOPG-substrate, 25°C , $25\% \text{ RH}$). In order to minimize the perturbations due to the AFM tip, the sample was scanned in the interruptive fashion over the course of several days, i.e., after capturing an image the scanning process was halted until it was time to capture

the next image. Every subsequent frame was readjusted relative to stationary surface defects such as terraces and pits to eliminate the 100 nm/h thermal drift of the sample. A complete study of the molecular diffusion by AFM will be presented elsewhere. Here, Fig. 3(d) demonstrates two time dependences of the mean-square displacement $\langle r_0^2(t) \rangle = 4D_{\text{therm}}t$ measured at 10-minute and 2-hour intervals and resulted in two diffusion coefficients $D_{\text{therm}} = 0.61 \pm 0.08 \text{ nm}^2/\text{s}$ and $D_{\text{therm}} = 0.10 \pm 0.03 \text{ nm}^2/\text{s}$, respectively. Since the interruptive scanning does not exclude the tip effect completely, the lower value is considered as an upper limit of the diffusion coefficient. In other words, without the tip-induced perturbations, molecules would move even slower ($D_{\text{therm}} \leq 0.10 \pm 0.03 \text{ nm}^2/\text{s}$).

The upper limit of the diffusion coefficient is relevant for the spreading kinetics as it gives a lower limit for the friction coefficient of a single PBA-brush molecule against the HOPG substrate as $\zeta_1 \geq (k_B T/D_{\text{therm}}) \cong 0.041 \pm 0.013 (Ns/m)$. This value can be used to verify the plug flow wherein the friction at the substrate is the dominant dissipation mechanism. For linear spreading [23], one writes the energy balance as $L \cdot \dot{L} \cdot \zeta_1 \cong S_0 \dot{\Sigma}$, where the left side represents the energy loss due to friction and the right side gives the energy gain due to spreading. Here, S_0 is the microscopic spreading parameter, $\Sigma = 7500 \pm 200 \text{ nm}^2$ is the averaged area per molecule, and $2L \cdot \dot{L} = D_{\text{spread}}$. For monolayers, S_0 depends on the film thickness and other molecular details that hinder its accurate evaluation [4]. For estimation purposes, we considered only the dominant term, i.e., the macroscopic spreading parameter S and set $S_0 \cong S$. Since mainly dispersion forces are involved in the interaction between the hydrocarbon polymer and the nonpolar substrate, $S \cong 2(\sqrt{\gamma_l^d \gamma_s^d} - \gamma_l)$ [24], where γ_l and γ_l^d are the surface energy and its dispersion component of PBA, and γ_s^d is the dispersion surface energy of HOPG. For the known $\gamma_l \cong 33 \text{ mJ/m}^2$, $\gamma_l^d \cong 23 \text{ mJ/m}^2$, and $\gamma_s^d \cong 80 \pm 10 \text{ mJ/m}^2$, one obtains $S \cong 20 \pm 6 \text{ mJ/m}^2$. This gives the molecular friction coefficient $\zeta_1 \cong (2S\Sigma/D_{\text{spread}}) = 0.08 \pm 0.03 (Ns/m)$, which is consistent with the lower limit $\zeta_1 \geq 0.041 \pm 0.013 (Ns/m)$.

As was noted above, the upper limit of the self-diffusion coefficient $D_{\text{therm}} < 0.10 \pm 0.03 \text{ nm}^2/\text{s}$ is noticeably lower than $D_{\text{induced}} = 1.3 \pm 0.1 \text{ nm}^2/\text{s}$ measured in the moving precursor film. This indicates that the diffusive motion in the precursor film has a different nature than the thermal diffusion of surface confined molecules and it is more likely induced by flow. This was verified by measuring the diffusion rate D_{induced} as a function of film velocity at different stages of the spreading process. Figure 4 shows that the molecular diffusion coefficient increases linearly with the film velocity, i.e., $D_{\text{induced}} \sim \dot{L}$. The origin of the molecular motion in the precursor film is still a subject for debates.

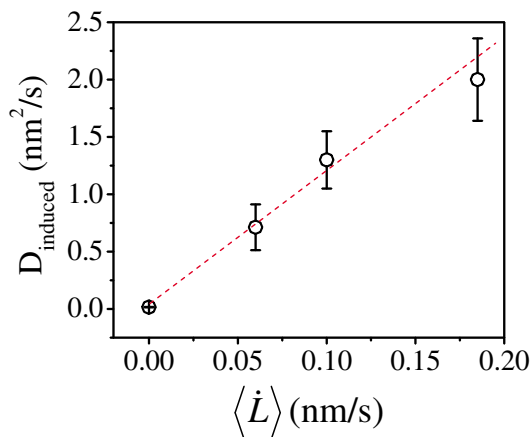


FIG. 4 (color online). The translational diffusion coefficient D_{induced} in the precursor film increases with the velocity of the film. This evidences the mechanically induced random-walk of molecules within the sliding film.

We believe that the random walk has its origin in random collisions of neighboring molecules as the dense monolayer is dragged over a solid substrate. This is reminiscent to the flow behavior of granular fluids for which an effective temperature can be calculated from the mechanically induced diffusion of particles [25–27]. Another explanation can be found in the heterogeneous structure of the substrate. Inevitable variations of the friction coefficient perturb the velocity field and thus cause collisions of spreading molecules leading to their diffusion. In order to check the effect of surface heterogeneities, we studied spreading on two HOPG substrates with different degrees of disordering due to the mosaic of monocrystal grains slightly disoriented with respect to each other: HOPG grade *A* with a mosaic spread of $0.4^\circ \pm 0.1^\circ$ and HOPG grade *B* with a mosaic spread $0.8^\circ \pm 0.2^\circ$. The diffusion coefficient on the more uniform HOPG-*A* was found to be significantly lower ($D_{\text{induced}} = 0.6 \text{ nm}^2/\text{s}$) than on the HOPG-*B* with larger density of defects ($D_{\text{induced}} = 1.3 \text{ nm}^2/\text{s}$). This suggests that the substrate heterogeneity influences the diffusive motion of molecules in sliding monolayers.

In summary, this study shows that the mass transport in the precursor film is due to the plug flow of polymer chains on a solid substrate with minor contribution from molecular diffusion. The slow diffusion does not contradict with the liquid state of the studied polymer [28]. It merely shows that the spreading proceeds faster than the thermal diffusion of brush molecules. The fluid nature of the sliding monolayer was confirmed with the transla-

tional and rotational diffusion of molecules within the precursor film. However, this diffusion is not a spontaneous one; it is induced by the sliding of a dense monolayer over a heterogeneous substrate.

This work was supported by the National Science Foundation (No. ECS 0103307 and No. DMR 0306787). M.R. acknowledges financial support from the NASA URETI on Bio-Inspired Materials No. NCC-1-02037

*Corresponding author.

- [1] P.G. de Gennes, *Rev. Mod. Phys.* **57**, 827 (1985).
- [2] A. M. Cazabat, *Contemp. Phys.* **28**, 347 (1987).
- [3] L. Leger and J. F. Joanny, *Rep. Prog. Phys.* **55**, 431 (1992).
- [4] A. M. Cazabat *et al.*, *J. Phys. Chem.* **94**, 7581 (1990).
- [5] M. Voué and J. de Coninck, *Acta Mater.* **48**, 4405 (2000).
- [6] R. Bruinsma, *Macromolecules* **23**, 276 (1990).
- [7] E. Ruckenstein, *Colloids Surf. A* **206**, 3 (2002).
- [8] H. M. Hardy, *Philos. Mag.* **38**, 49 (1919).
- [9] P. G. de Gennes and A. M. Cazabat, *C. R. Acad. Sci., Paris II* **310**, 1601 (1990).
- [10] F. Heslot and A. M. Cazabat, *Phys. Rev. Lett.* **62**, 1286 (1989).
- [11] T. E. Karis and G. W. Tyndall, *J. Non-Newtonian Fluid Mech.* **82**, 287 (1999).
- [12] X. Ma *et al.*, *Phys. Rev. E* **59**, 722 (1999).
- [13] D. Ausserré, A. M. Picard, and L. Leger, *Phys. Rev. Lett.* **57**, 2671 (1986).
- [14] C. Rivetti, M. Guthold, and C. Bustamante, *J. Mol. Biol.* **264**, 919 (1996).
- [15] S. S. Sheiko and M. Möller, *Chem. Rev.* **101**, 4099 (2001).
- [16] V. Percec *et al.*, *Nature (London)* **391**, 161 (1998).
- [17] A. Kiriya *et al.*, *J. Am. Chem. Soc.* **124**, 3218 (2002).
- [18] T. Hashimoto, A. Okumura, and D. Tanabe, *Macromolecules* **36**, 7324 (2003).
- [19] S. Villette *et al.*, *Physica (Amsterdam)*, **236A**, 123 (1997).
- [20] D. Glick, P. Thiansathaporn, and R. Superfine, *Appl. Phys. Lett.* **71**, 3513 (1997).
- [21] S. S. Sheiko *et al.*, *Macromolecules* **34**, 8354 (2001).
- [22] K. Matyjaszewski, J. Xia, *Chem. Rev.* **101**, 2921 (2001).
- [23] For radial spreading, one has to add a logarithmic prefactor.
- [24] J. Israelachvili, *Intermolecular and Surface Forces* (Academic Press, San Diego, CA, 1992), 2nd ed.
- [25] H. M. Jaeger, S. R. Nagel, and R. P. Behringer, *Rev. Mod. Phys.* **68**, 1259 (1996).
- [26] H. A. Makse and J. Kurchan, *Nature (London)* **415**, 614 (2002).
- [27] G. D'Anna *et al.*, *Nature (London)* **424**, 909 (2003).
- [28] C. M. Mate and B. Marchon, *Phys. Rev. Lett.* **85**, 3902 (2000).